crystals

MDPI

Article

Nanostructured Iron Oxides: Structural, Optical, Magnetic, and Adsorption Characteristics for Cleaning Industrial Effluents

Suriyaprabha Rajendran [1,*], Shivraj Gangadhar Wanale [2], Amel Gacem [3], Virendra Kumar Yadav [4], Inas A. Ahmed [5], Jari S. Algethami [6,7], Shakti Devi Kakodiya [8], Timsi Modi [9], Amnah Mohammed Alsuhaibani [10], Krishna Kumar Yadav [11] and Simona Cavalu [12,*]

1 School of Nanosciences, Central University of Gujarat, Gandhinagar 302030, India
2 School of Chemical Sciences, Swami Ramanand Teerth Marathwada University, Nanded 431606, India
3 Department of Physics, Faculty of Sciences, University 20 Août 1955, Skikda 21000, Algeria
4 Department of Microbiology-Biosciences, School of Liberal Arts & Sciences, Mody University, Laxmangarh, Sikar 332311, India
5 Department of Chemistry, Faculty of Science, King Khalid University, Abha 62224, Saudi Arabia
6 Department of Chemistry, College of Science and Arts, Najran University, Najran 11001, Saudi Arabia
7 Promising Centre for Sensors and Electronic Devices (PCSED), Najran University, Najran 11001, Saudi Arabia
8 School of Bioscience, Rani Durgavati Vishwavidyalaya, Jabalpur 482001, India
9 Department of Environment Science, P P Savani University, Surat 394125, India
10 Department of Physical Sport Science, College of Education, Princess Nourah bint Abdulrahman University, Riyadh 11671, Saudi Arabia
11 Faculty of Science and Technology, Madhyanchal Professional University, Ratibad, Bhopal 462044, India
12 Faculty of Medicine and Pharmacy, University of Oradea, P-ta 1 Decembrie 10, 410087 Oradea, Romania
* Correspondence: sooriyarajendran@gmail.com (S.R.); aaw-wad@kku.edu.sa (S.C.)

Abstract: Globally, efforts are being made to upgrade and improvise the current wastewater treatment technologies. Industrial wastewater is being generated exponentially, owing to the expansion in chemical industries and civilizations necessitating remediation to prevent further environmental damage and lower associated human risks. In this work, iron oxide nanoparticles (IONPs) have been developed and employed as an efficient nanocatalyst for heavy metal adsorption via the chemical route. The shape, absorbance optical, crystal phase, and magnetization of as-prepared magnetic nanostructures were characterized using XRD (X-ray diffraction), UV-Vis (ultraviolet-visible), HRTEM (High-resolution transmission electron microscopy), FTIR (Fourier transfer infrared spectroscopy), and VSM. Further, the adsorption ability of iron oxide to remove the bulk metallic elements considering cadmium (Cd), lead (Pb), zinc (Zn), chromium (Cr), copper (Cu), and nickel (Ni), present in industrial effluents, were studied. The Maghemite Fe_2O_3 crystal phase having an R-3c group is observed in the XRD results. An identical shape of spherical nanostructures is determined using TEM including ≈21 nm for pure Fe_2O_3. A removal % was studied by using ICP-OES, and showed a Cr (61.2%), Cd (98%), Cu (66%), Ni (64%), Zn (97%), and Pb (98%) removal ability. The application of such monitored nanomaterials to effluent cleaning and sewage discharge emitted via labs and petrochemical industries could be expanded.

Keywords: iron oxides; magnetic ability; adsorption; industrial effluents; environmental applications

check for updates

Citation: Rajendran, S.; Wanale, S.G.; Gacem, A.; Yadav, V.K.; Ahmed, I.A.; Algethami, J.S.; Kakodiya, S.D.; Modi, T.; Alsuhaibani, A.M.; Yadav, K.K.; et al. Nanostructured Iron Oxides: Structural, Optical, Magnetic, and Adsorption Characteristics for Cleaning Industrial Effluents. *Crystals* **2023**, *13*, 472. https://doi.org/10.3390/cryst13030472

Academic Editors: Zhaohui Li and Yi Zhou

Received: 17 January 2023
Revised: 1 March 2023
Accepted: 2 March 2023
Published: 9 March 2023

Copyright: © 2023 by the authors. Licensee MDPI, Basel, Switzerland. This article is an open access article distributed under the terms and conditions of the Creative Commons Attribution (CC BY) license (https://creativecommons.org/licenses/by/4.0/).

1. Introduction

Wastewater is produced in massive quantities by dye, textile, and other chemical-based industries, and it contains dangerous transitional ions, raw components (aromatics), and intermediate products, in addition to colors [1,2]. Such toxic waste-generating sectors are constantly looking into improved, more environmentally friendly methods of detoxifying wastewater pollutants [3,4]. Many scientists and researchers have concentrated on material engineering at the nanoscale because dye production, textile preparation, and dye industries are currently required to eliminate toxic substances due to hydrocarbonic chemicals

and stabled dye pigments including soluble hazardous components of sludges [5]. Water scarcity has become an inevitable concern for mankind owing to the release of improperly treated wastewater containing hazardous organic and inorganic contaminants into the surface water, which has impacted living beings and the environment overall [6,7]. Globalization of petrochemical and raw ingredient companies emitting aromatic cyclic hydrocarbons, as well as hazardous intermediates and molecular, inorganic, metallic, and biological pollutants discovered in wastewater, has raised serious concerns about water quality and related discharge criteria [8]. Inorganic heavy metals and molecular dye components impose a detrimental effect on the environment by releasing toxicants into the water, soil, and air. As a result, scientists and research professionals were intrigued by employing efficient desired approaches for introducing the ecosystem-based challenges mainly related to chemical and fabric productions [9,10]. Numerous studies have been conducted in the industry and academia to remediate toxic heavy metal ions from wastewater or effluents. Ni, Pb, Cd, Cr, Zn, and Cu form most toxic minerals present within wastewater [11–13]. These toxic discharged metals can cause dangerous diseases in animals, plants, and environmental components such as water, air, and soils, and hence the solution to these issues has become an important topic for the several researchers. Recently, scientific groups have praised the adsorption of chemically reactive ions or elements in wastewater employing semiconductors, photocatalysis, and bioremediation techniques. High-weighted metals and poisonous compounds have been removed utilizing a range of methods, including physicochemical, biological, and electrochemical processes, as well as the use of appropriate nanocatalysts [14,15]. Moreover, metals, metal oxides, and hybrid nanostructures have been employed to improve the chemo-adsorption and catalytic efficiency by modifying the morphological and structural orientations of such materials [13,16,17]. The increased active surface sites in the nano-sized stable catalysts, which include semiconducting TiO_2, ZnO, iron oxides, and 2D nanomaterials like graphene and graphene oxides, make it easier to chemosorb heavy ions or metals [18,19]. Given the rapid electron recombination in holes and electrons and efficient electron transport, these modified structures are commonly found. Although many nanocatalysts were researched for the elimination of toxic substances from effluents with induced catalytic performance, stability, and functionality, there is still much to be accomplished in the field of hybrid catalytic nanostructure synthesis and engineering. The most common in situ bioremediation and chemical reduction methods have been observed to compete with iron-based nanostructures. In comparison to other metal oxide remediation strategies, iron oxide nanoparticles offer better potential in toxic metal adsorption owing to their infinite surface area, better magnetic character, and precise diameters [20,21]. The iron oxide NPs have a strong superparamagnetic and magnetic susceptibility, therefore employed in the fabrication of magnetic nano-adsorbents. Furthermore, magnetic NPs are involved in an external magnetic field but lose their magnetism on the removal of the external field; thus, recycling their recovery is found to be easier and more convenient in our study. These features make iron oxides realistic nanocatalysts to remove heavy metals from pollutants. With the intent of adsorbing hazardous metals generated from industries, specific selective adsorption characteristics of iron oxide were studied. In nanoscience and associated advances, iron oxide in a controlled and functionalized form was employed to maximize adsorption efficiency. Interestingly, the catalysts' capability to adsorb contaminants is influenced by the structure, surface, crystal phase, and type of the intended chemical and organic contaminants [11]. In this study, a controlled IONP was constructed using a straightforward Sonochemical method [22,23]. After morphological and structural confirmation, the stabilized iron oxide nanostructures were used as an efficient nanocatalyst to absorb pollutants from the sample. According to the results provided by ICP-OES technology, the Zn, Cr, Cd, Ni, and Cu, with the Pb, were selectively eliminated from industrial wastewater.

2. Materials and Methods

Chemicals such as Iron (III) chloride ($FeCl_3$), Ferrous sulfate heptahydrate ($FeSO_4 \cdot 7H_2O$), and Sodium Hydroxide (NaOH), required in the study were obtained from Sigma Aldrich.

2.1. Preparation of Iron Oxides

The sonochemical method to synthesize magnetic NPs was conducted under defined magnetic stirring, using 0.1 M of $FeCl_3$ with $FeSO_4 \cdot 7H_2O$ (50 mL) (Sigma Aldrich, St. Louis, MO, USA, 99%) was employed as a precursor. The precursors in the molar ratio of 1:1 (Solutions A and B) were mixed in distilled water (30 mL). Solutions A and B were homogenized at 650 rpm on a magnetic stirrer, following which a reduction reaction was conducted by dropwise addition of ≈12 mL of 0.01 M NaOH in the reaction mixture, which was around 12 mL until the production of black precipitate in the reaction mixture. In addition, 9–11 values of optimized pH for reaction formulation were maintained using NaOH under room temperature. A Digital Ultrasonic bath QLDUC2.5 (QuickLab, Chennai, India) with 120 W of ultrasonic power operated at 40 kHz was used during the synthesis procedure. The formation of black precipitate during the end of the process directed a complete synthesis of iron oxides NP. Further, the synthesized magnetic nanoparticles were separated using a hand magnet, followed by multiple cleaning of suitable polar solvents (ethanol) which was then treated at 25 °C. Finally, the prepared magnetic nano powder was characterized for its structural and morphological features using advanced instruments.

2.2. Fundamental Techniques Used in Characterizations

Fundamental instruments employed to characterize the magnetic nanoparticles are as follows: Spectro 2060 plus UV-Vis Spectroscopy spectrophotometer (200–800 nm) for assessing the optical absorption study. However, the X-ray Diffraction of Bruker (Billerica, MA, USA), having λ = 0.15408 nm at a scanning rate of 0.02°/s, was used to identify crystal phases; the morphological and surface images of the magnetic particles analyzed using FE-SEM, JSM-7800F JEOL), and high-resolution transmission electron microscopy (HRTEM) JEOL, JEM 2100F. The function group of the possible composition was determined by applying FTIR, Perkin Elmer, Waltham, MA, USA) in the range of 4000–400 cm^{-1} [24].

3. Result and Discussions

3.1. Crystalline Confirmations: XRD Study

The XRD data of the iron oxide is examined particularly for determining the crystal phase of prepared magnetic samples. The XRD profile is shown in Figure 1. The obtained powder diffraction data were compared with the database containing references (using Match software). The Fe_2O_3 maghemite crystal phase is confirmed with the highest peak positions at 30.54, 32.09, 35.98, and 63.23 2θ values were well matched with PDF no. of 96-901-2693 (Figure 1). The fitted XRD data revealed crystalline phases of the magnetic nanoparticles (shown in figure with PDF numbers) corresponding to (2 2 0), (104), (3 1 1), (4 0 0) crystallographic planes and 2.9, 2.7, 2.4, and 1.4 (Å) d-spacing, respectively [25]. There are various phases of magnetic nanostructures, and after matching the diffraction date with the database in Match software, we found the maghemite Fe_2O_3 phase [26]. These diffraction angles and d-spacing (Å) also matched well with the JSPDS card no. (JCPDS code: 01-076-7166) for the maghemite phase, the standard diffraction angles for maghemite found to be 30.241, 35.630, 43.284, 53.733 57.271, and 62.925 2θ values which corresponded to 2.953, 2.517, 2.088, 1.704, 1.607, and 1.475 d-space (Å), respectively. However, the standardized values for magnetite ferrites were found to be (30.095, 2.967), (35.422, 2.532), (43.052 2.099), (53.391, 1.714), (56.942 1.615), and (62.515 1.484) (JCPDS code: 01-076-7166). Therefore, maghemite Fe_2O_3 NPs were confirmed for the as-prepared samples, which have a closed diffraction angles and d-spacing values that match with standard data as compared to other ferrite states.

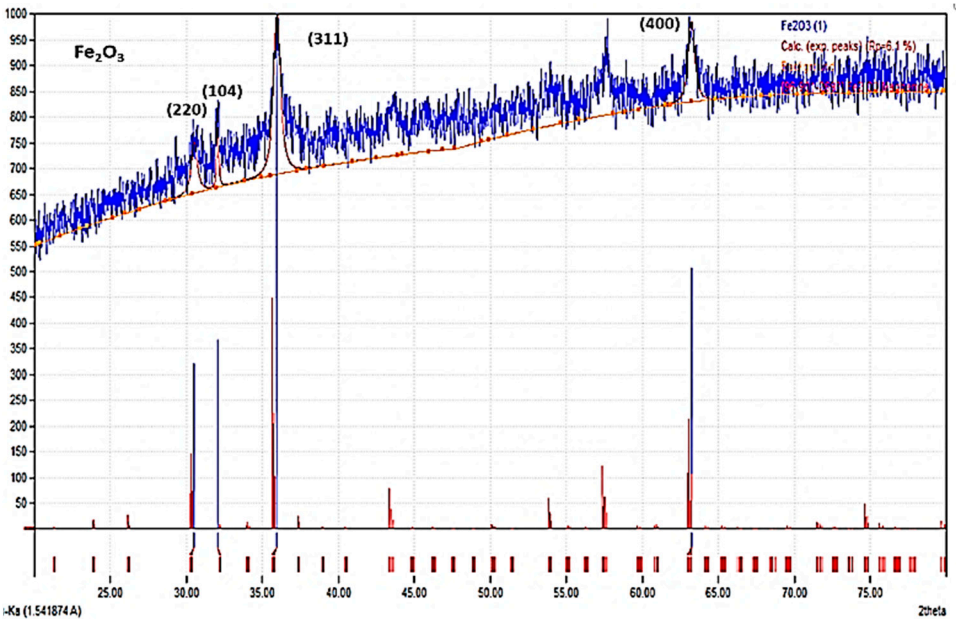


Figure 1. XRD Profile of iron oxides (Fe_2O_3).

3.2. Optical Absorbance Study (UV-Vis Spectra)

The optical absorbance feature for the IONPs in the ranges of 200–800 nm wavelength showed in Figure 2. The UV-Vis spectrophotometer technique is a fundamental tool to determine the synthesis of nonmaterials because of particular optical absorbances spectra. A certain position of absorption spectra gives a clear information for the formation of metal and metal oxide nanoparticles at fixed wavelength (26). The absorbance spectrum shows a primarily visible absorption wavelength at around 366 nm, confirming the formation of iron oxide, which is synthesized under the Sonochemical method at RT. The observed absorbance peak occurs due to the valance band-free electronic excitation of the IONPs under the electromagnetic spectrum [27].

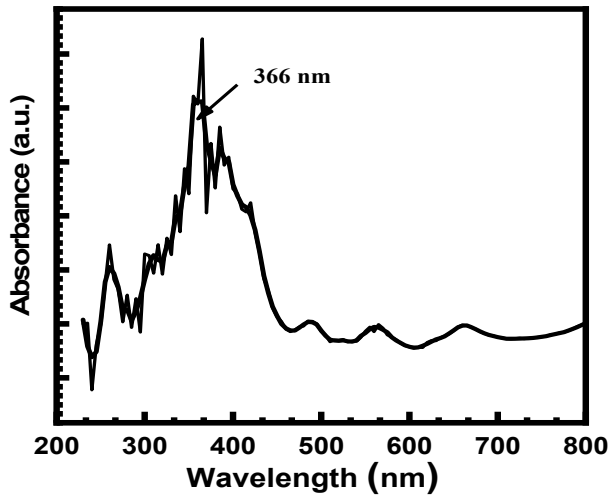


Figure 2. UV-Vis spectra of IONPs.

3.3. Functional Group Confirmations: FTIR Analysis

Figure 3 shows the functional group of the magnetic nanoparticles at room temperature in the region of 4000–400 cm^{-1}, which was determined using FT-IR spectroscopy. The vibrionic frequency associated with the Fe-, O-, and OH-linked functional groups is confirmed by characteristic vibrational modes in FTIR spectra. In the bare magnetite lattice, the vibrational stretching of the Fe-O bond is clearly visible as prominent spectra near

551 cm^{-1}. However, a peak at around 3400 and 1627 cm^{-1} suggests that the vibrational modes for the hydroxyl (OH) assembly may be due to the adsorbed water molecules (H_2O) [28].

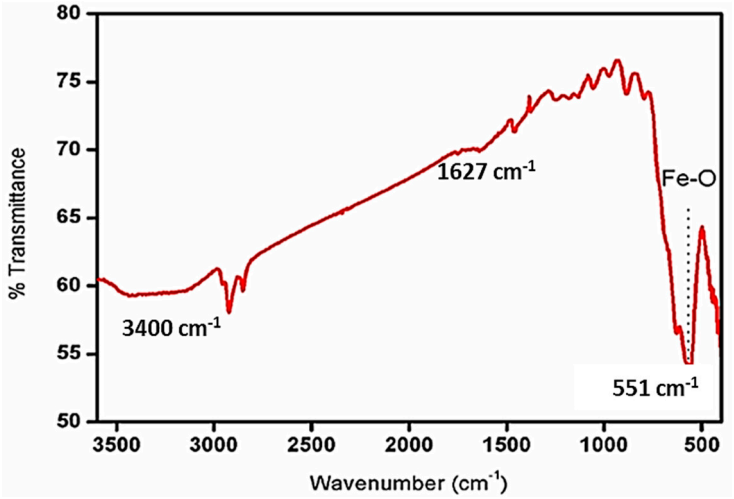


Figure 3. FTIR Spectra of IONPs.

3.4. Morphological Studies: HRTEM Investigation

A HRTEM image of iron oxide nanostructures confirming the morphology and elemental compositions is displayed in Figure 4. The microscopy indicates that the nanoparticle is spherical, with a minimal particle diameter of roughly 10 nm and a maximal average dimension of 20 nm (Figure 4a). The d-spacing has also been measured and shown to be approximately 0.24 nm (Figure 4b), which was additionally validated by XRD analysis. The Selected Area Diffraction Pattern (SAED) of the produced nanoparticles demonstrated that it is partly crystal in form (Figure 4d). However, after employing a Sonochemical approach, the electron microscopic figure depicts some aggregation since these nanoparticles of metal oxide prefer to associate more with one another, so the capping agent was not included in the process [29]. The resulting object's EDX plot suggests the spikes of Fe and O in acceptable element proportions (see Figure 4c).

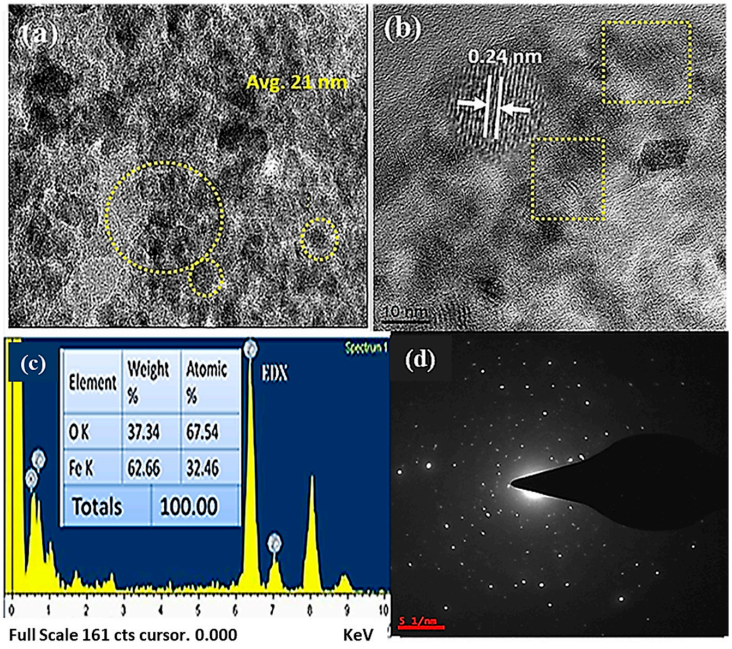


Figure 4. (**a**) Shape and size for IONPs by TEM. (**b**) HRTEM image for F3O4 NPs, (**c**) EDX spectra. (**d**) The SAED pattern of IONPs.

3.5. Vibrating Sample Magnetometer (VSM) Study of Iron Oxides NPs

VSM measures the magnetism quality of particular substances (Figure 5). A used electromagnetic field H is affected more by magnetism M, which could be calculated using the Langevin equation mentioned below [30]:

$$M = M_s\left(Cothy\frac{1}{Y}\right), \text{and}$$
$$Y = \frac{mH}{kBT}$$

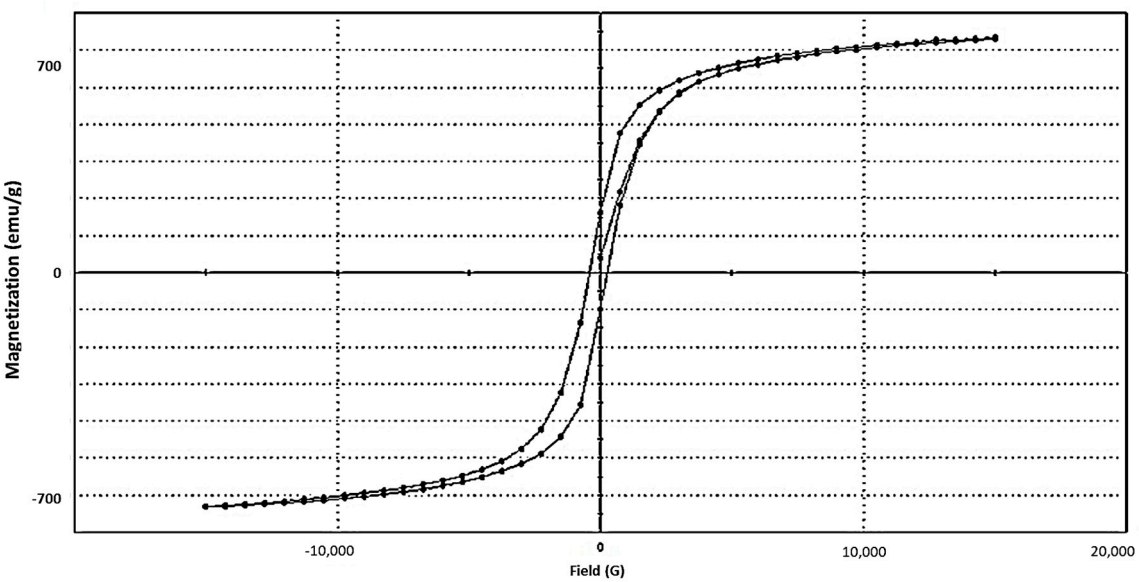


Figure 5. VSM measurement of IONPs.

M_s is the saturation magnetism and kB stands for the Boltzmann constant. The magnetic behavior of IONPs also depends upon the morphologies of the nanostructures. The shown hysteresis displays a superparamagnetic character of generated magnetic materials at 25 °C, revealing characteristic lenient ferromagnetics [30,31].

4. Remediation of Industrial Effluents

Synthesized Fe_2O_3 samples are employed to adsorb the bulk metals discharged by the chemical resources due to their strong magnetic character. The sample effluent was directly collected from dye manufacturing industries before being circulated to a common effluent treatment plant (CETP) for their treatment using conventional methods. The S1–S5 denotes the different points of a plant (five sites in total were chosen for collecting samples) and the initial concentration was determined using AAS (Table 1). The removal of pathogens, organic contaminants, and heavy metals was carried out using synthesized nanoparticles owing to their heavy metal removal efficiency attributed to the unique properties of the material, which includes magnetic impacts, large surface-to-volume ratio, shape, and size (under 40 nm).

Table 1. The concentration (mg/L) of identified metallic ions present in the effluents.

Elements	S-1 Conc.	S-2 Conc.	S-3 Conc.	S-4 Conc.	S-5 Conc.
Cr	0.423	0.311	0.287	0.316	0.117
Ni	0.013	0.020	0.017	0.008	0.039
Cd	0.001	0.003	0.006	0.004	0.001
Cu	0.05	0.032	0.652	0.083	0.054
Pb	0.013	0.01	0.015	0.063	0.005
Zn	1.670	1.34	0.096	0.87	0.56

The atomic absorption spectroscopy, AAS (model: ICE3300; make: Thermo Scientific) and ICP OES were performed to measure high-weight ions available initially within a sample. An aqueous solution of iron oxide nanoparticles with known concentration was prepared to conduct a heavy metal removal study. The experiment was carried out for 45 min in a rotary shaker at 32 °C under ideal conditions (25 °C and 1 atm). The specimen was repeated at 15 min intervals by separating IONPs using an external magnetic field. AAS and ICP OES (model: 7300 DV; make: Perkin Elmer) were used to further analyze the heavy metal content in relation to the starting concentration. The experiment was repeated with three different concentrations of IONPs (10 mg, 20 mg, and 30 mg). The elimination potential of the used sample is determined by applying equation as denoted below [13]:

$$R(\%) = \frac{C_0 - C_e}{C_0} \times 100$$

R (%) denotes to removal percentage, C_0 is the preliminary Conc. (mg/L), and C_e is the concentration (mg/L).

4.1. Removal of Heavy Metals Using Iron Oxide Nanoparticles

The samples were collected and stored by adding nitric acid. Before testing using the ICP or AAS technique, we need to form complete ionization of metal ions because in bonded form (complex), metal cannot be detected by these techniques with exact concentration. Hence, we treated sample with the nitric acid so that the metal ions could be ionized and the ionic metal could be easily tested by ICP or AAS. The toxic elements were analyzed employing AAS and ICP-OES. AAS was considered for sensing the Cr and Ni, whereas cadmium, copper, lead, and zinc that were found at low concentrations were detected using ICP–OES. The AAS technique is used for knowing the initial metal ion concentration for the makeup samples (S1–S5); however, for the determining removal percentage of metal ions using our samples, only the ICP technique is performed. Table 1 shows the amount of hazard ionic elements present under the chosen effluent.

Heavy metal concentrations in industrial wastes were found, and they were eliminated by employing IONPs. Mixed sewage was used in the study to eliminate the heavy metals, and it was discovered that their extraction efficiency (R%) grew as the IONP content was raised. Since the R% was calculated every 15 min, the concentration of sample catalysts in mg (10 mg, 20 mg, and 30 mg) (not mass) was used to determine the ideal amount for the removal. The experiment was performed using a conical flask (250 mL) at 150 rpm.

4.2. Chromium (Cr) Removal

A necessary mineral called chromium may cause cancer if consumed in excess (0.05 mg/L). The oxidation number of the metals affects how poisonous Cr combinations are. Cr exists within trivalent conditions in both animals and humans. Because toxic metals are not biodegradable and are found in dyestuff as a chromophoric component, they build up in the body's key organs and cause a variety of clinical manifestations [32]. IONPs were used to remove excess Cr, and the degradation rate was determined. A range of 0.117–0.423 mg/L of Cr was discovered. An improved R% was obtained at the dosage of 30 mg IONPs, according to the elimination investigation, as shown in Figure 6.

Three distinct doses of IONPs were used to remove the Cr. The maximum removal was evaluated and reported to be 61.2% applying 30 mg of IONPs, which produced an improved outcome compared to the other two concentrations.

4.3. Cadmium (Cd) Removal

Nearly all groundwater samples contain a quantity of toxic metals, notably cadmium. Wastewater is frequently used as a dyeing medium. In collected samples, Cd ranges from 0.001–0.006 mg/L, which does not specify an instant threat to lifeforms. In higher concentrations, it can damage the kidney and cause itai-itai disease [13,33]. Iron oxides

were used to absorb the highest quantity of cadmium, and it was discovered that 98% was eliminated in under 30 min.

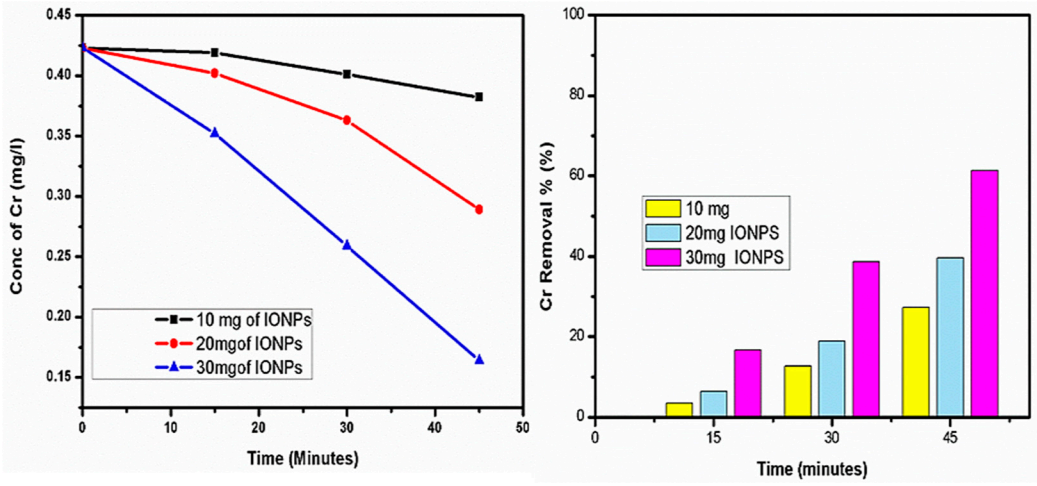


Figure 6. Removal % of Cr using IONPs at different concentrations and their removal.

The absorption of cadmium by IONPs is shown in Figure 7, and the elimination of sewage sludge that included a low amount of cadmium was also verified by the preliminary and final concentrations of the component in the sewage. The elimination of toxic Cd elements at 30 mg of IONP is what causes the level to decrease, according to the amount versus time graph plot.

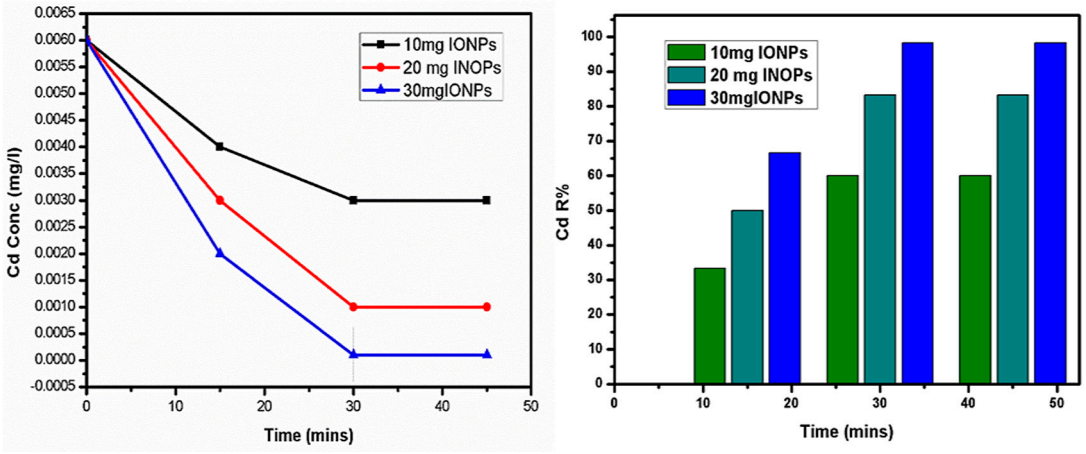


Figure 7. Removal of Cd using IONPs at different concentrations and their removal%.

4.4. Elimination of Copper (Cu)

A copper concentration from 0.083 to 0.032 mg/L was observed. Excessive Cu concentrations cause gastrointestinal problems as well as a green line on the gums. Cu buildup in the abdomen is linked to the disorder heptoleuticular degeneration as a hereditary abnormality. Hazardous metallic reduction might also result in the recovery of groundwater for commercial and home usage [12]. Cu subtraction is accomplished by applying magnetic particles, showing a max. 66% elimination and 24% (minimum). Increasing the dose for IONPs provides an increased deduction percentage (Figure 8).

4.5. Nickel (Ni) Removal

Medicinal symptoms including skin inflammations, renal disorder, and lung blockage are caused by the excess of Ni ions [11,34]. The concentration of Ni was observed in the range of 0.039–0.008 mg/L within the tested water solution. Nickel subtraction was attained at a max. of 94% in 30 mg of sample (30 min), Figure 9. The remaining dosages possess

comparably lower efficiency for the same study. The removal work was carried out for max. 45 min to optimize the adsorption mechanism, which showed ideal conditions at 30 min reaction.

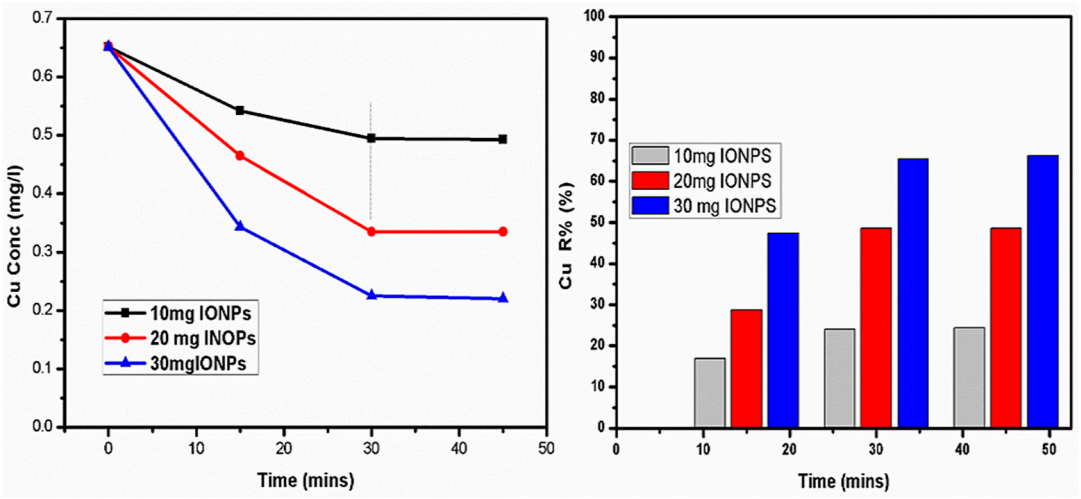


Figure 8. Removal of Cu using IONPs at different concentrations and their removal%.

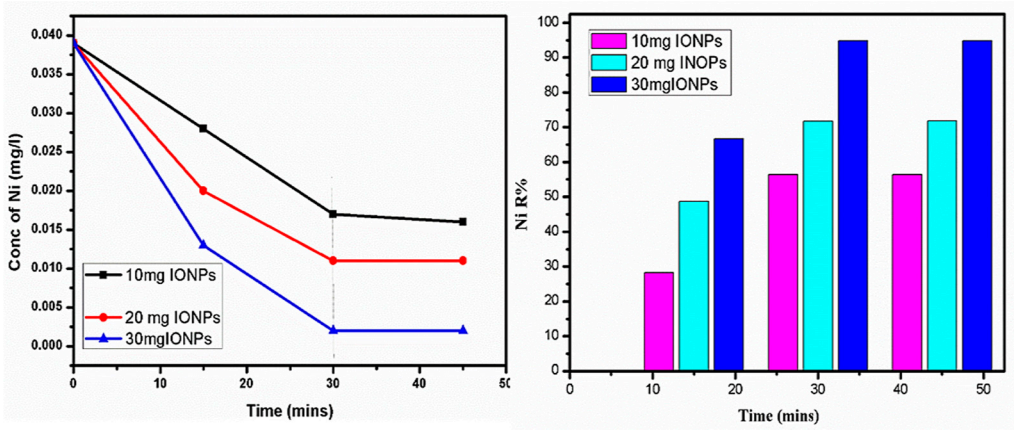


Figure 9. Removal of Ni using IONPs at different concentrations and their removal%.

4.6. Zn Elimination Study

The amount of zinc, a vital trace element, ranged between 1.67 to 0.096 mg/L. The current investigation found reduced Zn concentrations throughout all specimens. Increased Zn concentrations could induce astringent flavor and opalescence in groundwater [35,36]. An elimination of Zn was accomplished using three distinct IONP doses. Figure 10 demonstrates the decrease in ion concentrations with the passage of time. Taking 30 mg of INOPs, the discharge percentage was estimated to be 97% after 30 min. The content versus time figure shows that Zn is present at first, but disappears within 30 min.

4.7. Lead (Pb) Removal

The lead appearance in the tested water ranges from 0.063 to 0.005 mg/L. Pb's harm to ocean organisms, notably fishes and humans, is widely known. Pb poison in humans could result in lassitude, gastrointestinal issues, anemia, mental retardation, and hypertension [37,38].

Figure 11 reveals a considerable sample amount with adsorption time—the various quantity of samples displayed a maximum (98%) and minimum (34%) removal at 30 and 10 mg concentrations.

Adsorption, which is typically used for the filtration of water and wastewater, is a mass transfer process where contaminants in a solution are carried to a solid adsorbent

according to the ion exchange, hydrophobic interaction, and H bonding theories. Iron oxide hydroxyl is frequently generated in aqueous solutions as a result of the atomic Fe's coordination with water. Iron oxide surface atoms coordinate with compounds that give away lone-pair electrons by acting as Lewis acids. These hydroxyl radicals can interact with bases or acids because they are amphoteric. Heavy metals from wastewater could be removed by the adsorption of these ions based on the physicochemical characteristics of magnetic particles and as a result of chemisorption. Generally, metal ions in an aqueous solution can exist as steady moieties or hydrolyze in order to produce a string of single and multiple hydroxyl assemblies, shown in the reaction below.

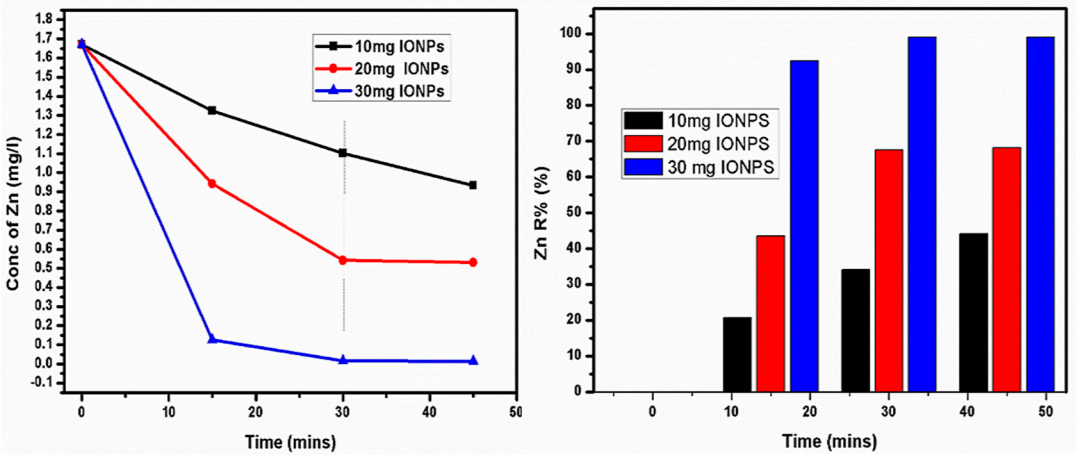


Figure 10. Removal of Zn using IONPs at different concentrations and their removal%.

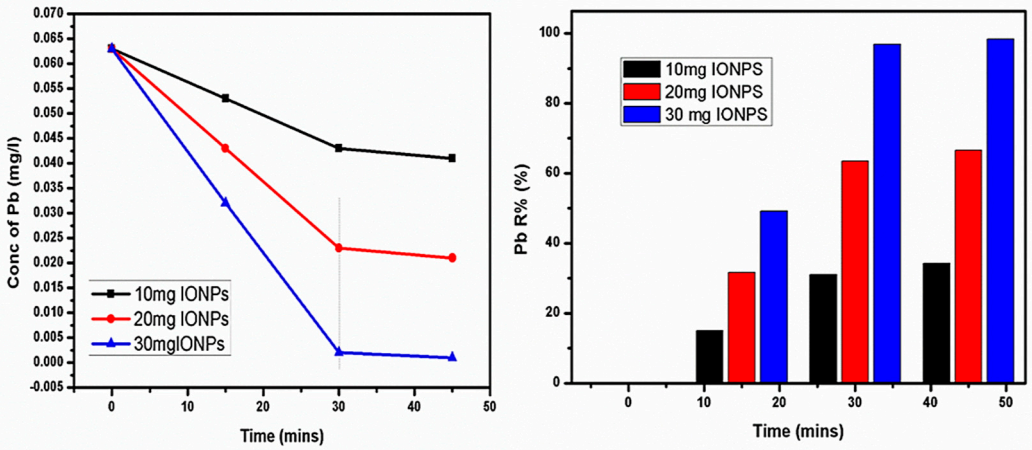


Figure 11. Removal of Pb using IONPs at different concentrations and their removal%.

$$M^{+} + nH_2O \leftrightarrow M(OH)n(m - n^2 + nH^{+})$$

M simply used to mention metal. The mechanism could be displayed as given below:

$$H_2O + Fe - O^{-} \leftrightarrow Fe - OH \leftrightarrow Fe - OH_2^{+}$$

Therefore, electrostatic interaction may be the valid reason for the adsorption of metallic ions towards the negatively enriched surfaces of the Fe_2O_3 nanoparticles. These research findings were also supported by the reported experimental and theoretical simulations, which are a fundamental procedure to carrying out nanoscopic and modern technical studies [39–43].

5. Conclusions

Iron oxide nanostructures were prepared to employ the simplest and most cost-effective Sonochemical pathway. Shape, sizes, and magnetic behavior of manufactured iron

oxides were confirmed using advanced instruments considering as XRD, UV-Vis, FTIR, HR-TEM, and VSM instruments. The optical absorption peak located at 360.15 nm revealed successful preparation for maghemite Fe_2O_3 nanostructures associated with XRD sizes having a maximum 21.3 nm average crystal size. HRTEM results depict an almost spherical shape of 20 nm magnetic NPs. The heavy metals were adsorbed from the industrial effluents using a maximum of 30 mg of iron oxides and the removal % was studied by ICP-OES, demonstrating a Cr (61.2%), Ni (64%), Cu (66%), Zn (97%), Cd (98%), and Pb (98%) removal. It can be concluded that the maximum 30 mg of IONPs was found more effective for Cd, Zn, and Pb, with over 97% removal from industrial waste. Such a heavy metal removal process could be applied for other metal extractions from various textiles, dye industries, and chemical laboratories using structurally modified IONPs.

Author Contributions: Conceptualization, S.R., K.K.Y. and V.K.Y.; Data curation, S.D.K., A.G. and S.G.W.; methodology, S.R., V.K.Y. and S.C.; validation, S.R. and K.K.Y.; formal analysis, S.R., S.G.W. and A.G. resources, S.R., A.M.A. and S.C.; writing—original draft preparation, S.R., S.D.K., T.M. and K.K.Y.; writing—review and editing, S.R., S.G.W., I.A.A. and K.K.Y.; supervision, S.R. and S.C.; project administration S.C. and K.K.Y. Funding acquisition, K.K.Y., S.C. and S.R.; Investigation, S.R. and J.S.A.; Software's, S.R. and T.M.; Visualization, J.S.A. and S.R. All authors have read and agreed to the published version of the manuscript.

Funding: The reported work is supported financially by Dean of Science and Research at King Khalid University via the General Research Project (grant number. R.G.P.1/320/43). The authors are thankful to the Deanship of Scientific Research at Najran University for funding the present research, by Research Groups Funding program grant code (NU/RG/SERC/12/45). Princess Nourah bint Abdulrahman University Researchers Supporting Project number (PNURSP2023R65), Princess Nourah bint Abdulrahman University, Riyadh, Saudi Arabia. The APC for this article was funded by University of Oradea, Romania.

Acknowledgments: The authors are grateful to the Dean of Science and Research at King Khalid University for making financial support available. The authors are thankful to the Deanship of Scientific Research at Najran University for funding the present research, by Research Groups Funding program grant code (NU/RG/SERC/12/45). Princess Nourah bint Abdulrahman University Researchers Supporting Project number (PNURSP2023R65), Princess Nourah bint Abdulrahman University, Riyadh, Saudi Arabia. The APC for this article was funded by University of Oradea, Romania. Authors are obliged to SNS, central university of Gujarat, Gandhinagar-203830 India for providing infrastructure for performing experimental work.

Conflicts of Interest: There is no competing interests by the authors.

References

1. Yadav, V.K.; Yadav, K.K.; Gacem, A.; Gnanamoorthy, G.; Ali, I.H.; Khan, S.H.; Jeon, B.-H.; Kamyab, H.; Inwati, G.K.; Choudhary, N.; et al. A novel approach for the synthesis of vaterite and calcite from incense sticks ash waste and their potential for remediation of dyes from aqueous solution. *Sustain. Chem. Pharm.* **2022**, *29*, 100756. [CrossRef]
2. Kumar, P.; Inwati, G.K.; Mathpal, M.C.; Maze, J.; Swart, H.C. Recent Advances on Ferrites Nanomaterial's as Photocatalyst for Environment. In *Advances in Nanostructured Materials. Materials Horizons: From Nature to Nanomaterials*; Swain, B.P., Ed.; Springer: Singapore, 2022. [CrossRef]
3. Kumar, P.; Kumar, A.; Rizvi, M.A.; Moosvi, S.K.; Krishnan, V.; Duvenhage, M.; Roos, W.; Swart, H. Surface, optical and photocatalytic properties of Rb doped ZnO nanoparticles. *Appl. Surf. Sci.* **2020**, *514*, 145930. [CrossRef]
4. Inwati, G.K.; Kumar, P.; Swart, H.C. Multifunctional properties of hybrid semiconducting nanomaterials and their applications. In *Electronic and Optical Materials, Nanoscale Compound Semiconductors and Their Optoelectronics Applications*; Elsevier: Amsterdam, The Netherlands, 2022; pp. 315–350. [CrossRef]
5. Inwati, G.K.; Yadav, V.K.; Ali, I.H.; Vuggili, S.B.; Kakodiya, S.D.; Solanki, M.K.; Yadav, K.K.; Ahn, Y.; Yadav, S.; Islam, S.M.; et al. 2D Personality of Multifunctional Carbon Nitrides towards Enhanced Catalytic Performance in Energy Storage and Remediation. *Appl. Sci.* **2022**, *12*, 3753. [CrossRef]
6. Chopra, H.; Bibi, S.; Singh, I.; Hasan, M.M.; Khan, M.S.; Yousafi, Q.; Baig, A.A.; Rahman, M.; Islam, F.; Bin Emran, T.; et al. Green Metallic Nanoparticles: Biosynthesis to Applications. *Front. Bioeng. Biotechnol.* **2022**, *10*, 874742. [CrossRef]
7. Rajendran, S.; Inwati, G.K.; Yadav, V.K.; Choudhary, N.; Solanki, M.B.; Abdellattif, M.H.; Yadav, K.K.; Gupta, N.; Islam, S.; Jeon, B.-H. Enriched Catalytic Activity of TiO_2 Nanoparticles Supported by Activated Carbon for Noxious Pollutant Elimination. *Nanomaterials* **2021**, *11*, 2808. [CrossRef] [PubMed]

8. Marimuthu, S.; Antonisamy, A.J.; Malayandi, S.; Rajendran, K.; Tsai, P.-C.; Pugazhendhi, A.; Ponnusamy, V.K. Silver nanoparticles in dye effluent treatment: A review on synthesis, treatment methods, mechanisms, photocatalytic degradation, toxic effects and mitigation of toxicity. *J. Photochem. Photobiol. B Biol.* **2020**, *205*, 111823. [CrossRef]
9. Rahman, M.; Wadnerkar, N.; English, N.J.; MacElroy, J. The influence of Ti- and Si-doping on the structure, morphology and photo-response properties of α-Fe_2O_3 for efficient water-splitting: Insights from experiment and first-principles calculations. *Chem. Phys. Lett.* **2014**, *592*, 242–246. [CrossRef]
10. Bibi, I.; Nazar, N.; Ata, S.; Sultan, M.; Ali, A.; Abbas, A.; Jilani, K.; Kamal, S.; Sarim, F.M.; Khan, M.I.; et al. Green synthesis of iron oxide nanoparticles using pomegranate seeds extract and photocatalytic activity evaluation for the degradation of textile dye. *J. Mater. Res. Technol.* **2019**, *8*, 6115–6124. [CrossRef]
11. Inwati, G.K.; Mehetre, S.; Ameta, R.K.; Kumar, P.; Swart, H.C.; Yadav, V.K.; Makwana, B.A.; Kakodiya, S.D.; Gnanamoorthy, G. *Smart Supercapacitors—A New Perspective*; Elsevier: Amsterdam, The Netherlands, 2023; pp. 159–176. Available online: https://www.sciencedirect.com/science/article/pii/B9780323905305000277 (accessed on 27 January 2023). [CrossRef]
12. Ebrahim, S.E.; Sulaymon, A.H.; Alhares, H.S. Competitive removal of Cu^{2+}, Cd^{2+}, Zn^{2+}, and Ni^{2+} ions onto iron oxide nanoparticles from wastewater. *Desalin. Water Treat.* **2016**, *57*, 20915–20929. [CrossRef]
13. Vaclavikova, M.; Misaelides, P.; Gallios, G.; Jakabsky, S.; Hredzak, S. Removal of cadmium, zinc, copper and lead by red mud, an iron oxides containing hydrometallurgical waste. *Stud. Surf. Sci. Catal.* **2005**, *155*, 517–525. [CrossRef]
14. Julkapli, N.M.; Bagheri, S.; Bee, S.; Hamid, S.B.A. Recent Advances in Heterogeneous Photocatalytic Decolorization of Synthetic Dyes. *Sci. World J.* **2014**, *2014*, 692307. [CrossRef]
15. Cavalu, S.; Simon, V. Microstructure and bioactivity of acrylic bone cements for prosthetic surgery. *J. Optoelectron. Adv. Mater.* **2006**, *8*, 1520–1523.
16. Inwati, G.; Kumar, P.; Roos, W.; Swart, H.; Singh, M. UV-irradiation effects on tuning LSPR of Cu/Ag nanoclusters in ion exchanged glass matrix and its thermodynamic behaviour. *J. Alloys Compd.* **2020**, *823*, 153820. [CrossRef]
17. Inwati, G.K.; Kumar, P.; Roos, W.; Swart, H. Thermally induced structural metamorphosis of ZnO: Rb nanostructures for antibacterial impacts. *Colloids Surf. B Biointerfaces* **2020**, *188*, 110821. [CrossRef] [PubMed]
18. Darkwah, W.K.; Ao, Y. Mini Review on the Structure and Properties (Photocatalysis), and Preparation Techniques of Graphitic Carbon Nitride Nano-Based Particle, and Its Applications. *Nanoscale Res. Lett.* **2018**, *13*, 388. [CrossRef] [PubMed]
19. Modi, S.; Inwati, G.K.; Gacem, A.; Saquib Abullais, S.; Prajapati, R.; Yadav, V.K.; Syed, R.; Alqahtani, M.S.; Yadav, K.K.; Islam, S.; et al. Nanostructured Antibiotics and Their Emerging Medicinal Applications: An Overview of Nanoantibiotics. *Antibiotics* **2022**, *11*, 708. [CrossRef]
20. Kong, L.; Lu, X.; Bian, X.; Zhang, W.; Wang, C. Constructing Carbon-Coated Fe_3O_4 Microspheres as Antiacid and Magnetic Support for Palladium Nanoparticles for Catalytic Applications. *ACS Appl. Mater. Interfaces* **2011**, *3*, 35–42. [CrossRef]
21. Mishra, M.; Chun, D.-M. α-Fe 2 O 3 as a photocatalytic material: A review. *Appl. Catal. A Gen.* **2015**, *498*, 126–141. [CrossRef]
22. Hassanjani-Roshan, A.; Vaezi, M.R.; Shokuhfar, A.; Rajabali, Z. Synthesis of iron oxide nanoparticles via sonochemical method and their characterization. *Particuology* **2011**, *9*, 95–99. [CrossRef]
23. Shafi, K.V.P.M.; Ulman, A.; Yan, X.; Yang, N.-L.; Estournès, C.; White, H.; Rafailovich, M. Sonochemical Synthesis of Functionalized Amorphous Iron Oxide Nanoparticles. *Langmuir* **2001**, *17*, 5093–5097. [CrossRef]
24. Inwati, G.K.; Rao, Y.; Singh, M. Thermodynamically induced in Situ and Tunable Cu Plasmonic Behaviour. *Sci. Rep.* **2018**, *8*, 3006. [CrossRef] [PubMed]
25. Hei, S.; Jin, Y.; Zhang, F. Fabrication of γ-Fe_2O_3Nanoparticles by Solid-State Thermolysis of a Metal-Organic Framework, MIL-100(Fe), for Heavy Metal Ions Removal. *J. Chem.* **2014**, *2014*, 546956. [CrossRef]
26. Kim, E.H.; Lee, H.S.; Kwak, B.K.; Kim, B.-K. Synthesis of ferrofluid with magnetic nanoparticles by sonochemical method for MRI contrast agent. *J. Magn. Magn. Mater.* **2005**, *289*, 328–330. [CrossRef]
27. Chaki, S.H.; Malek, T.J.; Chaudhary, M.D.; Tailor, J.P.; Deshpande, M.P. Magnetite Fe_3O_4 nanoparticles synthesis by wet chemical reduction and their characterization. *Adv. Nat. Sci. Nanosci. Nanotechnol.* **2015**, *6*, 035009. [CrossRef]
28. Mohammadikish, M. Hydrothermal synthesis, characterization and optical properties of ellipsoid shape α-Fe_2O_3 nanocrystals. *Ceram. Int.* **2014**, *40*, 1351–1358. [CrossRef]
29. Lassoued, A.; Dkhil, B.; Gadri, A.; Ammar, S. Control of the shape and size of iron oxide (α-Fe_2O_3) nanoparticles synthesized through the chemical precipitation method. *Results Phys.* **2017**, *7*, 3007–3015. [CrossRef]
30. Deotale, A.J.; Nandedkar, R.V.; Sinha, A.K.; Upadhyay, A.; Mondal, P.; Srivastava, A.K.; Deb, S.K. Effect of isochronal annealing on phase transformation studies of iron oxide nanoparticles. *Bull. Mater. Sci.* **2015**, *38*, 599–606. [CrossRef]
31. Abdo, N.I. Comparative Study between Magnetite Nanoparticles and Magnetite/Silver as a Core/Shell Nanostructure. *Adv. Nanoparticles* **2021**, *10*, 115–122. [CrossRef]
32. Kumar, A.S.K.; Jiang, S.-J.; Tseng, W.-L. Effective adsorption of chromium(vi)/Cr(iii) from aqueous solution using ionic liquid functionalized multiwalled carbon nanotubes as a super sorbent. *J. Mater. Chem. A* **2015**, *3*, 7044–7057. [CrossRef]
33. Mohamed, H.S.; Soliman, N.; Abdelrheem, D.A.; Ramadan, A.A.; Elghandour, A.H.; Ahmed, S.A. Adsorption of Cd^{2+} and Cr^{3+} ions from aqueous solutions by using residue of Padina gymnospora waste as promising low-cost adsorbent. *Heliyon* **2019**, *5*, e01287. [CrossRef]
34. Boujelben, N.; Bouzid, J.; Elouear, Z.; Feki, M. Retention of nickel from aqueous solutions using iron oxide and manganese oxide coated sand: Kinetic and thermodynamic studies. *Environ. Technol.* **2010**, *31*, 1623–1634. [CrossRef] [PubMed]

35. Ahmed, A.; Ayad, M.I.; Eledkawy, M.A.; Darweesh, M.; Elmelegy, E.M. Removal of iron, zinc, and nickel-ions using nano bentonite and its applications on power station wastewater. *Heliyon* **2021**, *7*, e06315. [CrossRef] [PubMed]
36. Chaudhry, S.A.; Khan, T.A.; Ali, I. Adsorptive removal of Pb(II) and Zn(II) from water onto manganese oxide-coated sand: Isotherm, thermodynamic and kinetic studies. *Egypt. J. Basic Appl. Sci.* **2016**, *3*, 287–300. [CrossRef]
37. Wang, B.; Yu, J.; Liao, H.; Zhu, W.; Ding, P.; Zhou, J. Adsorption of Lead (II) from Aqueous Solution with High Efficiency by Hydrothermal Biochar Derived from Honey. *Int. J. Environ. Res. Public Health* **2020**, *17*, 3441. [CrossRef]
38. Yang, X.; Xu, G.; Yu, H. Removal of lead from aqueous solutions by ferric activated sludge-based adsorbent derived from biological sludge. *Arab. J. Chem.* **2019**, *12*, 4142–4149. [CrossRef]
39. Cavalu, S.; Antoniac, I.V.; Fritea, L.; Mates, I.M.; Milea, C.; Laslo, V.; Vicas, S.; Mohan, A. Surface modifications of the titanium mesh for cranioplasty using selenium nanoparticles coating. *J. Adhes. Sci. Technol.* **2018**, *32*, 2509–2522. [CrossRef]
40. Cavalu, S.; Simon, V.; Goller, G.; Akin, I. Bioactivity and antimicrobial properties of pmma/Ag_2O acrylic bone cement collagen coated. *Dig. J. Nanomater. Biostructures* **2011**, *6*, 779–790.
41. Cavalu, S.; Simon, V. Proteins adsorption to orthopaedic biomaterials: Vibrational spectroscopy evidence. *J. Optoelectron. Adv. Mater.* **2007**, *9*, 3297–3302.
42. Simon, V.; Cavalu, S.; Simon, S.; Mocuta, H.; Vanea, E.; Prinz, M.; Neumann, M. Surface functionalisation of sol–gel derived aluminosilicates in simulated body fluids. *Solid State Ion.* **2009**, *180*, 764–769. [CrossRef]
43. Ormanci, O.; Akin, I.; Sahin, F.; Yucel, O.; Simon, V.; Cavalu, S.; Goller, G. Spark plasma sintered Al_2O_3–YSZ–TiO_2 composites: Processing, characterization and in vivo evaluation. *Mater. Sci. Eng. C* **2014**, *40*, 16–23. [CrossRef]

Disclaimer/Publisher's Note: The statements, opinions and data contained in all publications are solely those of the individual author(s) and contributor(s) and not of MDPI and/or the editor(s). MDPI and/or the editor(s) disclaim responsibility for any injury to people or property resulting from any ideas, methods, instructions or products referred to in the content.